Journal of Solid State Chemistry 243 (2016) 18–22

Contents lists available at ScienceDirect

Journal of Solid State Chemistry

journal homepage: www.elsevier.com/locate/jssc

Zig-zag magnetic ordering in honeycomb-layered $Na_3Co_2SbO_6$

Cheryl Wong [a], Maxim Avdeev [b], Chris D. Ling [a,*]

[a] School of Chemistry, The University of Sydney, Sydney, NSW 2006, Australia
[b] Bragg Institute, B87, Australian Nuclear Science and Technology Organisation, Locked Bag 2001, Kirrawee DC, NSW 2232, Australia

ARTICLE INFO

Article history:
Received 3 May 2016
Received in revised form
9 July 2016
Accepted 31 July 2016
Available online 3 August 2016

Keywords:
Layered oxides
Honeycomb
Magnetic structure
Neutron diffraction
Zig-zag

ABSTRACT

$Na_3Co_2SbO_6$ is a layered oxide with a hexagonal O3-type structure, in which CdI_2-type edge-sharing MO_6 octahedral layers are intercalated by Na. The MO_6 octahedral layer in turn adopts a honeycomb ordering pattern of magnetic ($S=3/2$) Co^{2+} sites surrounding isolated non-magnetic Sb^{5+} sites. Magnetic susceptibility measurements show that $Na_3Co_2SbO_6$ orders antiferromagnetically below $T_N=8.3$ K, with an effective magnetic moment of 5.22 μ_B (indicating a strong orbital contribution above the expected spin-only value of 3.87 μ_B). While a honeycomb arrangement of magnetic cations could, in principle, support a co-operative long-range-ordered magnetic structure in which all nearest neighbors are antiferromagnetic with respect to one another, symmetry analysis of low-temperature neutron powder diffraction data shows that it instead adopts a partially frustrated 'zig-zag' ordering in which 2/3 of nearest-neighbor interactions are ferromagnetic and 1/3 are antiferromagnetic. The low Néel temperature and Weiss constant of $\theta = 2.2$ K underlines the presence of significant frustration of the expected strong superexchange interactions among Co^{2+}.

1. Introduction

Transition-metal oxides that are capable of intercalating small mobile ions such as Li^+ and Na^+ have been intensively studied for their electrochemical properties [1–3], but their magnetic properties remain relatively unexplored. Those with CdI_2-type oxide layers such as $LiCoO_2$ [4,5], which are the most interesting for metal-ion battery cathode applications, have quasi two-dimensional triangular arrays of transition metals which are not conducive to long-range magnetic ordering. Nevertheless, in many cases they still show interesting properties, the most notable example being bulk superconductivity in $Na_xCoO_2{\cdot}yH_2O$ [6,7].

When one-third of the transition metal cations are replaced with non-magnetic cations with significantly higher charges, such as Te^{6+}, Sb^{5+} or Bi^{5+}, an ordered hexagonal honeycomb lattice of magnetic cations results [8]. This is shown in Fig. 1 for the title compound $Na_3Co_2SbO_6$ [9,10], which adopts the O3 interlayer stacking sequence polytype [11] in which the Na cations occupy octahedral interstices.

The honeycomb topology supports long-range magnetic order of various types, including collinear nearest-neighbor antiferromagnetism (AFM). A significant number of such compounds have been synthesized, and although in the majority of cases only the lattice parameters have been reported, some have shown evidence for long-range magnetic ordering. In addition to the title compound, these include $Li_3Cu_2SbO_6$ [12], $Li_3Ni_2SbO_6$ [13,14], $Na_3Ni_2SbO_6$ [15], $Na_3Cu_2SbO_6$ [16], $Na_2Co_2TeO_6$ [9,17], $Na_2Ni_2TeO_6$ [17,18], $Na_2Cu_2TeO_6$ [19], $Li_3Ni_2BiO_6$ [20] and $Na_3Ni_2BiO_6$ [21]. Another class of honeycomb systems that has attracted recent attention are the iridates, notably the 'harmonic' Li_2IrO_3 series [22–24], the corner-sharing Ir^{5+} compound $Sr_3CaIr_2O_9$ [25], and Na_2IrO_3 [26,27].

To date, the only magnetic structures that have been reported for honeycomb materials comparable to that investigated in the present work are those of $Na_3Ni_2BiO_6$ [21] (determined experimentally) and $Na_3Ni_2SbO_6$ [15] (determined theoretically), both of which are reported to adopt a 'zig-zag' magnetic ground state. This is one of three ordered AFM ground states proposed for the honeycomb lattice, which are summarized in Fig. 2. It has been proposed that the 'zig-zag' model is the most likely structure for the archetypal $J = 1/2$ honeycomb lattice Na_2IrO_3 [26], based on *ab initio* calculations. The stable state for a $J = 3/2$ system such as $Na_3Co_2SbO_6$ has not been tested in this way.

Here, we present the results of the first low-temperature neutron diffraction studies of long-range magnetic structure for $Na_3Co_2SbO_6$. The oxidation state of Co is expected to be 2+ in both cases, noting that Sb is expected to be in its highest oxidation state of 5+. $Na_3Co_2SbO_6$ should therefore be a good candidate for long-range order given the relatively strong magnetic interactions typically observed among high-spin Co^{2+} ($S = 3/2$) ions directly bridged by oxide ions.

* Corresponding author.
E-mail address: chris.ling@sydney.edu.au (C.D. Ling).

http://dx.doi.org/10.1016/j.jssc.2016.07.032
0022-4596/

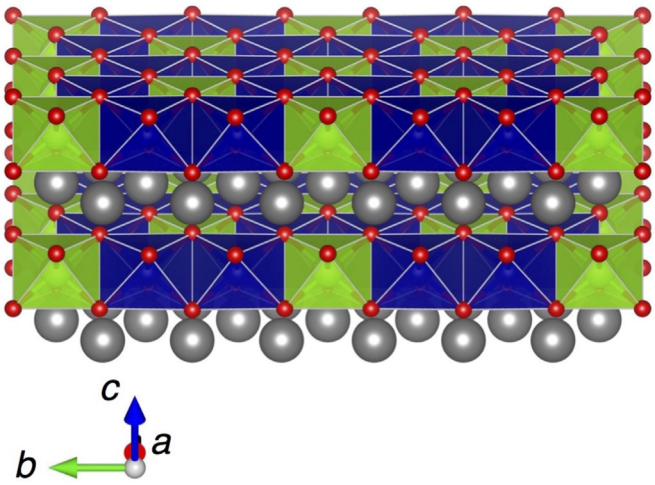

Fig. 1. Crystal structure of O3-type $Na_3Co_2SbO_6$ (monoclinic, S.G. $C2/m$). CoO_6 octahedra are blue, SbO_6 octahedra are green, O atoms are red and Na atoms are gray. The projection is chosen to highlight the 'honeycomb' distribution of Co around Sb in each layer. (For interpretation of the references to color in this figure legend, the reader is referred to the web version of this article.).

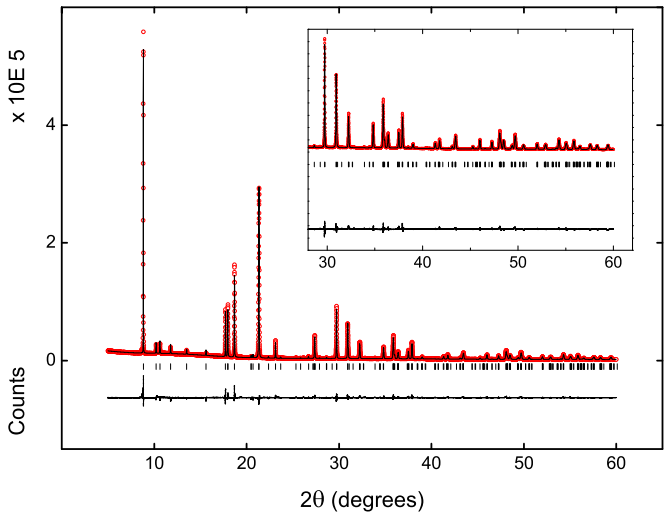

Fig. 3. Final Rietveld-refined fit to SXRD data (λ=0.825136(2) Å) for $Na_3Co_2SbO_6$. Observed (red dots), calculated (black line) and difference (blue line) patterns at low angles are shown. The inset highlights the high-angle data. (For interpretation of the references to color in this figure legend, the reader is referred to the web version of this article.).

2. Experimental section

$Na_3Co_2SbO_6$ was synthesized using conventional solid state methods from stoichiometric mixtures of Na_2CO_3 (Merck, 99.9%), Co_3O_4 (Sigma-Aldrich, <10 μm), and Sb_2O_3 (BDH Chemicals, 99%). The precursors were ground using an agate mortar and pestle, pressed into pellets, and sintered at 650 °C in air for 12 h. Following intermittent regrinding and pressing, the sample was calcined in air at 900 °C for 12 h.

The sample was confirmed to be single-phase using a PANalytical X'Pert PRO MPD X-ray powder diffractometer (XRD) in Bragg-Brentano geometry. The diffractometer was equipped with an unmonochromated Cu K_α source (λ_1 = 1.5406 Å, λ_2 = 1.5444 Å) operating at 45 kV/40 mA. Data were collected over an angular range of $10° < 2\theta < 80°$ at a rate of 0.028° s^{-1}.

Synchrotron X-ray powder diffraction (SXRD) patterns were collected on the Powder Diffraction beamline (10-BM-1) at the Australian Synchrotron. The beam was calibrated using the NIST LaB_6 660b standard to a wavelength λ = 0.825136(2) Å. Samples were loaded into 0.3 mm diameter glass capillaries and data collected using a MYTHEN microstrip detector over the 2θ range of $5° < 2\theta < 80°$, configured in Debye-Scherrer geometry. The crystal structure was refined using the Rietveld method as implemented in the GSAS program [28] with the EXPGUI front-end [29].

Temperature-dependent DC magnetic susceptibility, field-dependent magnetization and heat capacity measurements were made using a Quantum Design Physical Property Measurement System (PPMS). Susceptibility data were measured under zero field-cooled (ZFC) and field-cooled (FC) conditions in the temperature range of $2 < T < 300$ K using a coercive field of 0.1 T. Magnetization as a function of applied magnetic field was measured over the range of $-9 \le H \le 9$ T at constant temperatures of 2 and 40 K. Heat capacity measurements were collected over the temperature range of $2 < T < 50$ K under high vacuum.

Neutron powder diffraction (NPD) patterns were collected using neutrons of wavelength λ=2.4395 Å on the high-resolution powder diffractometer Echidna at the OPAL facility operated by ANSTO. A ~5 g powdered sample was loaded into a 9 mm diameter cylindrical vanadium can. Data were collected between 1.5 and 40 K using an 'orange' cryostat. The magnetic structure was analyzed using the Fullprof Suite [30] with the default neutron scattering lengths and the Co^{2+} magnetic form factor.

3. Results and discussion

The peaks in SXRD patterns of $Na_3Co_2SbO_6$ were all accounted for by a single phase, confirming the purity of the sample. The final Rietveld fits to these data are presented in Fig. 3. The refined unit cell is within the ranges of reported values in the literature, given in Table 1. The reported values vary significantly, which can be attributed to slight variations in the Na stoichiometry: reduced Na content weakens inter-layer interactions and expands the *c*-axis; while consequent partial oxidation of Co decreases the average cation size (and *vice versa*). The fact that our sample has both a smaller unit cell and a higher magnetic ordering temperature

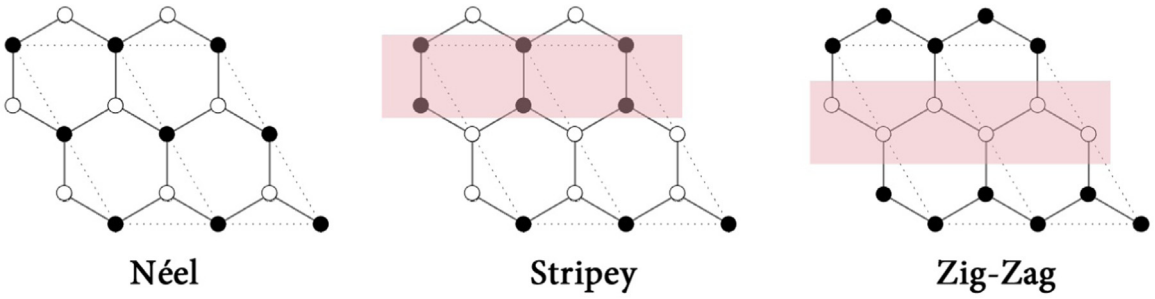

Fig. 2. Schematic illustrating possible AFM ordering patterns for magnetic cations on a honeycomb latticE (adapted from Liu et al. [26]). The black and white atoms indicate up and down spin, respectively. Dashed lines show the hexagonal unit cell of Na_2IrO_3.

Table 1
Experimental crystallographic and magnetic parameters for $Na_3Co_2SbO_6$ (monoclinic, S.G. *C*2/*m*) reported in the literature and in the present work (*).

a (Å)	*b* (Å)	*c* (Å)	*β* (°)	μ_{eff} (μ_B)	T_N (K)	*θ* (K)	Ref.
5.3681(2)	9.2849(4)	5.6537(2)	108.506(4)	4.9	4.4	−0.8	[9]
5.3627(2)	9.2790(1)	5.6514(2)	108.55(4)	–	–	–	[10]
5.35648(10)	9.28723(19)	5.65100(7)	108.358(1)	5.22	8.3	2.2	*

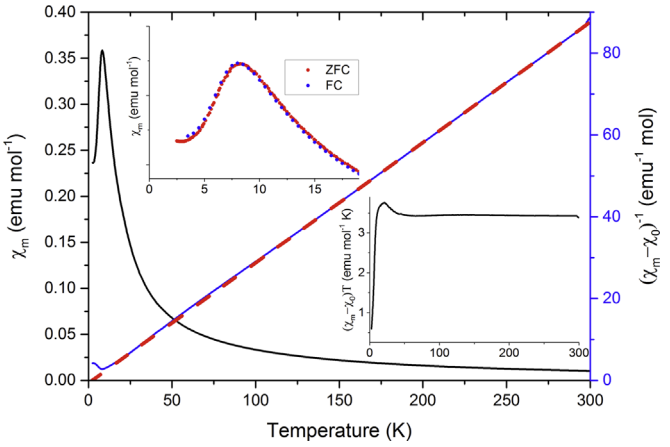

Fig. 4. Temperature-dependent DC magnetic susceptibility of $Na_3Co_2SbO_6$, measured in a coercive field of $H = 0.1$ T under zero-field cooled (black) and field-cooled (red) conditions. Data are only shown from 2 to 50 K to highlight the low-temperature magnetic ordering transition. (For interpretation of the references to color in this figure legend, the reader is referred to the web version of this article.).

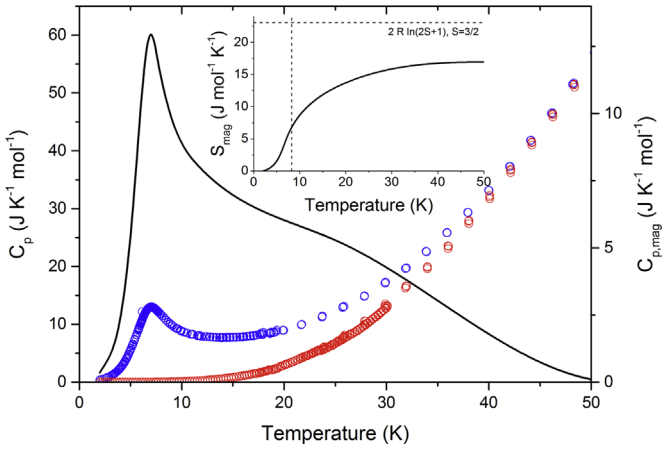

Fig. 6. Heat capacity data for $Na_3Co_2SbO_6$ (blue) and $Na_3Zn_2SbO_6$ (red) on the left-hand axis, with the magnetic contribution (black) on the right-hand axis. The inset shows the integrated magnetic entropy. (For interpretation of the references to color in this figure legend, the reader is referred to the web version of this article.).

(266.81 Å^3 and 8.3 K) than that of Viciu et al. [9] (267.22 Å^3 and 4.4 K) suggests that our sample is closer to the ideal stoichiometry. The volume difference of our sample compared to that of Politaev et al. [10] (266.61 Å^3) is not statistically significant.

The temperature-dependent susceptibility of $Na_3Co_2SbO_6$ is shown in Fig. 4. A magnetic transition is observed at 8.3 K, higher than the previously reported value of 4.4 K [9]; the difference may be due to varying sodium content, resulting in incomplete oxidation of Sb^{5+} accompanied by partial oxidation of Co^{2+}. The inverse temperature-dependent susceptibility shows linear Curie-Weiss behavior in the paramagnetic region, and ZFC/FC curves do not show divergence at T_N (Fig. 4, upper inset). A linear fit over the range 200–300 K with the modified Curie-Weiss law taking into account temperature-independent contribution yielded $\theta = 2.2$ K

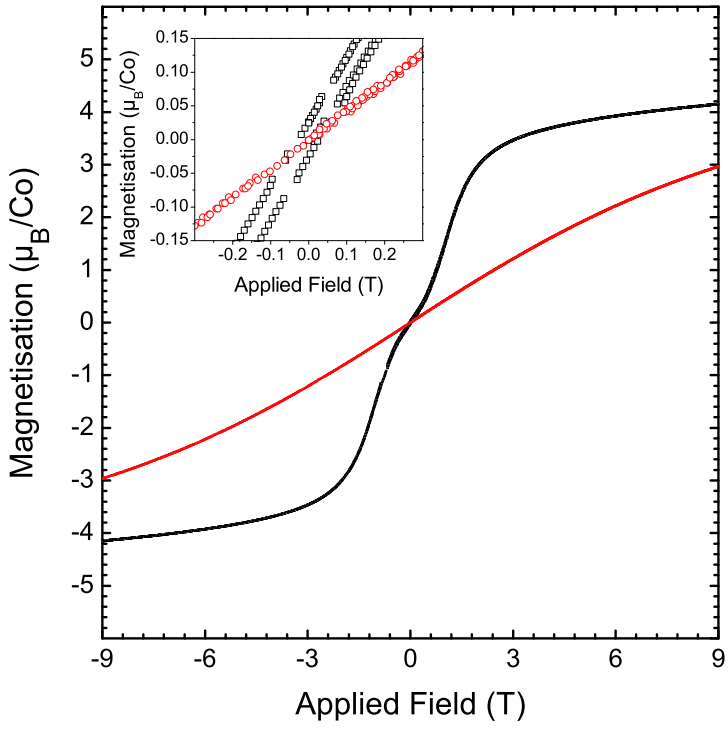

Fig. 5. Field-dependent magnetization of $Na_3Co_2SbO_6$ at 2 K (black) and 40 K (red), below and above the magnetic ordering transition respectively. The inset highlights the small hysteresis openings at low-fields. (For interpretation of the references to color in this figure legend, the reader is referred to the web version of this article.).

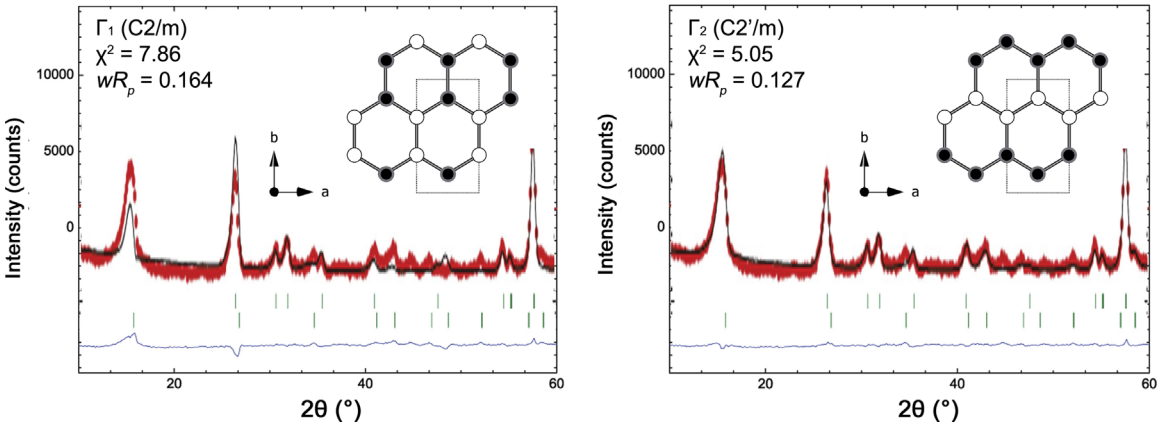

Fig. 7. Magnetic Rietveld refinement of each Γ_i model against NPD data for $Na_3Co_2SbO_6$ at 1.5 K. The weighted profile factor (wR_p) and the global χ^2 values are given for each irreducible representation. The observed (red dots), calculated (black line) and difference (blue line) patterns at low angles are shown. The upper and lower set of peak markers correspond to the nuclear and magnetic phase, respectively. The inset illustrates the orientation of collinear spins along the *c* axis (represented by black and white dots), with dashed lines indicating the unit cell. (For interpretation of the references to color in this figure legend, the reader is referred to the web version of this article.).

Table 2
Basis vectors for each irreducible representation at the four cobalt sites for $Na_3Co_2SbO_6$. The parentheses next to Γ_i indicate the Shubnikov group.

Cobalt Position **Site Coordinate**	**Co1** (0 $\frac{2}{3}$ 0)	**Co2** (0 $\frac{1}{3}$ 1)
Γ_1 (C2/m)	(1 0 0) (0 1 0) (0 0 1)	(−1 0 0) (0 −1 0) (0 0 −1)
Γ_2 (C2′/m)	(1 0 0) (0 1 0) (0 0 1)	(1 0 0) (0 1 0) (0 0 1)

and an effective magnetic moment of 5.22 μ_B. The value of the Weiss temperature suggests close competition between antiferromagnetic (AFM) and ferromagnetic (FM) interactions. This is supported by the evolution of the χT product as a function of temperature (Fig. 4, lower inset). On cooling below ~50 K, χT initially increases, which indicates onset of short range magnetic correlations of primarily FM character. However, below ~20 K, the χT behavior reverses, which signals the increasingly dominant contribution of the AFM interactions. The value of the effective moment reflects a significant contribution of unquenched orbital angular momentum, typical for Co^{2+} and in agreement with the previous report (Table 1 of Ref. [9]).

The 2 K isotherm (Fig. 5) reveals a narrow hysteresis loop opening, indicating that the material is magnetically 'soft'. This is consistent with the finely balanced Weiss temperatures. A small shoulder is observed, consistent with the results of Viciu et al. [9], who attributed it to a transition induced by the magnetic field. Although they did not investigate it further, they proposed that this may be characteristic of a spin-flop transition that broadens and moves to lower fields as T increases. The presence of such a shoulder is indicative of an AFM state with a small FM component. The 40 K isotherm is linear, suggesting that it is paramagnetic at this temperature. This result is consistent with the transition temperature determined from magnetic susceptibility.

The magnetic entropy associated with ordering was estimated from temperature-dependent heat capacity data (Fig. 6). The lattice component of the heat capacity was isolated by subtracting the heat capacity data for the non-magnetic analog Na_3Zn_2 SbO_6. The magnetic entropy ($S_{mag} = \int_0^T C_{p,mag}/T\, dT$) yielded a values of 15.8 J/mol K. This value is lower than the theoretical spin-only $2R\ln(2S+1) = 23.0$ J/mol K for Co^{2}+, consistent with the reduced ordered moment as seen by NPD (1.79 μ_B *vs.* the theoretical 3 μ_B, discussed below) (Fig. 7).

NPD data collected under zero applied field at 1.5 K revealed additional peaks that were not observed at 40 K, indicating a long-range ordered magnetic structure. This result is in agreement with magnetic susceptibility data, which suggested a transition temperature at 8.3 K. The magnetic peaks were indexed using the propagation vector of $k = (1/2, 1/2, 0)$. This corresponds to a commensurate magnetic structure, where the crystallographic unit cell is doubled along the *a* and *b* axes. The Fourier coefficients describing the magnetic ground state (Γ_m) can be decomposed into a linear combination of the basis functions of the one-dimensional irreducible representations (Γ_i), given by $\Gamma_m = 3\Gamma_1 + 3\Gamma_2$. The associated basis vectors for these irreducible representation are summarized in Table 2.

The spin arrangement in Γ_1 (C2/m) corresponds to the 'stripey' configuration, whereas Γ_2 (C2′/m) corresponds to 'zig-zag'. Each irreducible representation model was refined against NPD data at 1.5 K, allowing all three basis vectors to refine freely. The best agreement between experimental and calculated powder diffraction patterns was found to be for Γ_2, with a refined moment of [0.4 (2), 0.2(2), 1.10(8)] μ_B. Given that the (1 0 0) and (0 1 0) components of this refined moment were not statistically significant, they were set to zero for the final refinement – *i.e.*, only the (0 0 1) basis vector was used. The magnetic peaks in the NPD data also showed a slight asymmetric broadening, suggesting the presence of magnetic microstructural effects, which we modeled with an anisotropic size parameter based on platelet coherent domains.

The magnetic moment for Co^{2+} from this final refinement was 1.79(4) μ_B. This is smaller than the expected moment of 3 μ_B for an $S=3/2$ compound, suggesting incomplete ordering or magnetic frustration. A number of other layered honeycomb oxides also have 'zig-zag'-ordered magnetic ground states, including both Na_2IrO_3 [26] and $Na_3Ni_2BiO_6$ [21].

4. Conclusions

$Na_3Co_2SbO_6$ is the second honeycomb-type layered oxide of the type $Na_3M_2^{2+}A^{5+}O_6$ found to adopt the 'zig-zag' AFM structure at low-temperatures, after $Na_3Ni_2BiO_6$ [21]. $Na_3Ni_2SbO_6$ [15] has also been determined theoretically to adopt this ground state, which breaks hexagonal symmetry (although it should be noted that the symmetry was already lowered crystallographically to monoclinic above T_N). Surprisingly, no such oxide has been found to adopt the fully cooperative AFM Néel state (Fig. 2). This suggests a very fine balance between FM and AFM nearest-neighbor superexchange

interactions, increasing the relative influence of next-nearest-neighbor exchange in determining the ground state: in the 'zig-zag' state, 2/3 of nearest-neighbors and next-nearest-neighbors are AFM; while in the Néel state, all nearest-neighbors are AFM, but all next-nearest-neighbors are FM. Competition between FM and AFM exchange on both length scales results in magnetic frustration, consistent with the low $T_N = 8.3$ K and $\theta = 2.2$ K. In light of the complexity of the magnetic exchange interactions in honeycomb systems shown by, *e.g.*, Liu et al. for Na_2IrO_3, high-level *ab initio* calculations will be required to determine the precise nature of the situation for $Na_3Co_2SbO_6$.

Finally, it should be noted that the FM and AFM interactions in the 'zig-zag' AFM structure of $Na_3Co_2SbO_6$ do not occur among crystallographically equivalent Co-Co pairs, due to the symmetry lowering from hexagonal to monoclinic. It is therefore not strictly necessary to invoke competing interactions to explain 'zig-zag' order. However, the distances them are extremely similar: from synchrotron XRD data, at room temperature these distances are 3.09789(10) Å and 3.09559(14) Å respectively. (Our low temperature NPD data were collected at long wavelength and optimized for magnetic intensity, so did not yield reliable Co-Co distances.) This difference is clearly too small to treat the AFM pairs as isolated dimers. In future work it would be interesting to try to modify the structure and hence the balance between these competing interactions in order to try to stabilize the elusive Néel state, through chemical doping or the application of external applied pressure.

Acknowledgments

Financial support was provided for this projects by the Australian Research Council (Discovery Projects) and the Australian Institute of Nuclear Science and Technology (Grant no. DP150102863). SXRD data were collected with the technical assistance of Dr Justin Kimpton and the financial assistance of the Australian Synchrotron.

References

[1] K. Abraham, Solid State Ion. 7 (1982) 199–212.
[2] M.S. Whittingham, Chem. Rev. 104 (2004) 4271–4302.
[3] M.H. Han, E. Gonzalo, G. Singh, T. Rojo, Energy Environ. Sci. 8 (2015) 81–102.
[4] K. Mizushima, P. Jones, P. Wiseman, J. Goodenough, Mater. Res. Bull. 15 (1980) 783–789.
[5] J. Reimers, J. Dahn, J. Electrochem. Soc. 139 (1992) 2091–2097.
[6] K. Takada, H. Sakurai, E. Takayama-Muromachi, F. Izumi, R.A. Dilanian, T. Sasaki, Nature 422 (2003) 53–55.
[7] R. Schaak, T. Klimczuk, M.L. Foo, R.J. Cava, Nature 424 (2003) 527–529.
[8] M.A. Evstigneeva, V.B. Nalbandyan, A.A. Petrenko, B.S. Medvedev, A.A. Kataev, Chem. Mater. 23 (2011) 1174–1181.
[9] L. Viciu, Q. Huang, E. Morosan, H. Zandbergen, N. Greenbaum, T. McQueen, R. Cava, J. Solid State Chem. 180 (2007) 1060–1067.
[10] V. Politaev, V. Nalbandyan, A. Petrenko, I. Shukaev, V. Volotchaev, B. Medvedev, J. Solid State Chem. 183 (2010) 684–691.
[11] C. Delmas, C. Fouassier, P. Hagenmuller, Physica B+C 99 (1980) 81–85.
[12] J. Skakle, S.T. Tovar, A. West, J. Solid State Chem. 131 (1997) 115–120.
[13] E.A. Zvereva, M.A. Evstigneeva, V.B. Nalbandyan, O.A. Savelieva, S.A. Ibragimov, O.S. Volkova, L.I. Medvedeva, A.N. Vasiliev, R. Klingeler, B. Buechner, Dalton Trans. 41 (2012) 572–580.
[14] E.A. Zvereva, V.B. Nalbandyan, M.A. Evstigneeva, H.-J. Koo, M.-H. Whangbo, A. V. Ushakov, B.S. Medvedev, L.I. Medvedeva, N.A. Gridina, G.E. Yalovega, J. Solid State Chem. 225 (2015) 89–96.
[15] E. Zvereva, M. Stratan, Y. Ovchenkov, V. Nalbandyan, J. Lin, E. Vavilova, M. Iakovleva, M. Abdel-Hafiez, A. Silhanek, X. Chen, A. Stroppa, S. Picozzi, H. Jeschke, R. Valentí, A. Vasiliev, Phys. Rev. B 92 (2015) 144401.
[16] W. Schmidt, R. Berthelot, A. Sleight, M. Subramanian, J. Solid State Chem. 201 (2013) 178–185.
[17] R. Berthelot, W. Schmidt, A. Sleight, M. Subramanian, J. Solid State Chem. 196 (2012) 225–231.
[18] R. Sankar, I.P. Muthuselvam, G. Shu, W. Chen, S.K. Karna, R. Jayavel, F. Chou, CrystEngComm 16 (2014) 10791–10796.
[19] J. Xu, A. Assoud, N. Soheilnia, S. Derakhshan, H.L. Cuthbert, J.E. Greedan, M. H. Whangbo, H. Kleinke, Inorg. Chem. 44 (2005) 5042–5046.
[20] R. Berthelot, W. Schmidt, S. Muir, J. Eilertsen, L. Etienne, A. Sleight, M. A. Subramanian, Inorg. Chem. 51 (2012) 5377–5385.
[21] E.M. Seibel, J. Roudebush, H. Wu, Q. Huang, M.N. Ali, H. Ji, R. Cava, Inorg. Chem. 52 (2013) 13605–13611.
[22] H. Kobayashi, M. Tabuchi, M. Shikano, H. Kageyama, R. Kanno, J. Mater. Chem. 13 (2003) 957–962.
[23] M.J. O'Malley, H. Verweij, P.M. Woodward, J. Solid State Chem. 181 (2008) 1803–1809.
[24] T. Takayama, A. Kato, R. Dinnebier, J. Nuss, H. Kono, L.S.I. Veiga, G. Fabbris, D. Haskel, H. Takagi, Phys. Rev. Lett. 114 (2015).
[25] D.C. Wallace, T.M. McQueen, Dalton Trans. 44 (2015) 20344–20351.
[26] X. Liu, T. Berlijn, W.-G. Yin, W. Ku, A. Tsvelik, Y.-J. Kim, H. Gretarsson, Y. Singh, P. Gegenwart, J. Hill, Phys. Rev. B 83 (2011) 220403.
[27] J. Chaloupka, G. Jackeli, G. Khaliullin, Phys. Rev. Lett. 110 (2013).
[28] A. Larson, R. Von Dreele, Gen. Struct. Anal. Syst. (GSAS) (2000) 86–748.
[29] B. Toby, J. Appl. Crystallogr. 34 (2001) 210–213.
[30] J. Rodríguez-Carvajal, Physica B 192 (1993) 55–69.